Local Discriminant Direction Binary Pattern for Palmprint Representation and Recognition

Lunke Fei, Bob Zhang, *Member, IEEE*, Yong Xu, *Senior Member, IEEE*, Di Huang, *Member, IEEE*, Wei Jia, *Member, IEEE*, and Jie Wen

***Abstract*— Direction-based methods are the most powerful and popular palmprint recognition methods. However, there is no existing work that completely analyzes the essential differences among different direction-based methods and explores the most discriminant direction representation of a palmprint. In this paper, we attempt to establish the connection between the direction feature extraction model and the discriminability of direction features, and we propose a novel exponential and Gaussian fusion model (EGM) to characterize the discriminative power of different directions. The EGM can provide us with a new insight into the optimal direction feature selection of palmprints. Moreover, we propose a local discriminant direction binary pattern (LDDBP) to completely represent the direction features of a palmprint. Guided by the EGM, the most discriminant directions can be exploited to form the LDDBP-based descriptor for palmprint representation and recognition. Extensive experiment results conducted on four widely used palmprint databases demonstrate the superiority of the proposed LDDBP method over the state-of-the-art direction-based methods.**

***Index Terms*— Palmprint recognition, exponential and Gaussian fusion model, direction binary pattern, discriminant direction representation.**

I. Introduction

BIOMETRIC-BASED personal authentication has been widely applied in modern society due to its several advantages such as high-security, high-efficiency and user-friendliness [1], [2]. The widely used biometric traits include face, fingerprint, finger/palm/hand vein, iris, voice, gait, signature, and so on [3]. As a relatively new and promising biometric trait, a palmprint contains a number of highly discriminative features, including not only the obvious principal lines and wrinkles but also the significant ridge patterns and minutiae points, most of which are considered to be immutable to an individual [1], [4], [5]. Therefore, palmprint-based recognition technology has the potential to achieve a high accuracy and desirable performance [6]–[8].

So far, there have been various palmprint feature extraction and recognition methods in the literature [9]. For example, Huang *et al.* [10] and Palma *et al.* [11] extracted the principle lines of a palmprint for palmprint verification. Morales *et al.* [12] extracted the scale invariant feature transform (SIFT) based features for palmprint recognition. Dai *et al.* [13] proposed a multi-feature based high-resolution palmprint recognition method by fusing the principal lines and minutiae points of a palmprint. Ribaric *et al.* [14] proposed a Fisherpalm method for palmprint recognition by using Fisher's linear discriminant analysis. In addition, the study on machine-learning methods, such as subspace learning [14], [15] and sparse representation (SR) [16], for palmprint recognition has become active. For example, Guo *et al.* [16] proposed a palmprint recogniton method by using sparse representation. Zhang *et al.* [17] applied the collaborative representation (CR) scheme for palmprint identification. Imad *et al.* [18], [19] proposed a hybrid palmprint recognition method, which used 2-D PCA and 2-D LDA to form an ensemble discriminative dictionary of palmprint images, and then employed SR-based classifier for feature identification. Quite recently, the modern deep convolutional neural network is also applied for palmprint recognition [20]–[22]. For example, Izadpanahkakhk *et al.* [22] proposed a convolutional neural network and transfer learning fusion method to extract ROI and discriminative features for palmprint verification. Zhong *et al.* [8] systematically summarized state-of-the-art feature extraction and matching methods for palmprint recognition over the past decade. It is well known that a palmprint carries strong direction features along with its line and texture features. Moreover, direction feature is insensitive to illumination change [23]. For these reasons, more recently published methods [23]–[32] focused on the extraction of the direction features of a palmprint and achieved very promising recognition performance, which can be roughly classified into three categories, including the winner-take-all-based

Manuscript received August 15, 2018; revised October 13, 2018 and December 1, 2018; accepted January 1, 2019. Date of publication January 3, 2019; date of current version February 5, 2020. This work was supported in part by the National Natural Science Foundation of China under Grant 61702110, Grant 61673175, and Grant 61602540, in part by the Shenzhen Municipal Science and Technology Innovation Council under Grant JCYJ20170811155725434, and in part by the University of Macau Multi-Year Research Grant MYRG2018-00053-FST. This paper was recommended by Associate Editor H. Lu. *(Corresponding author: Bob Zhang.)*

L. Fei is with the School of Computer Science and Technology, Guangdong University of Technology, Guangzhou 510006, China (e-mail: flksxm@126.com).

B. Zhang is with the Department of Computer and Information Science, University of Macau, Macau 999078, China (e-mail: bobzhang@umac.mo).

Y. Xu and J. Wen are with the Bio-Computing Research Center, Harbin Institute of Technology (Shenzhen), Shenzhen 518055, China (e-mail: yongxu@ymail.com; jiewen_pr@126.com).

D. Huang is with the Beijing Advanced Innovation Center for Big Data and Brain Computing, Beihang University, Beijing 100191, China (e-mail: dhuang@buaa.edu.cn).

W. Jia is with the School of Computer and Information, Hefei University of Technology, Hefei 230009, China (e-mail: china.jiawei@139.com).

Color versions of one or more of the figures in this article are available online at http://ieeexplore.ieee.org.

Digital Object Identifier 10.1109/TCSVT.2019.2890835

methods, multiple-directions-based methods, and local direction statistics-based methods.

The winner-take-all rule based methods [26] generally extract the most dominant direction feature of palmprint. They are based on an underlying assumption that the pixels in a palmprint image belong to some lines and thus carry dominant directions. One of the most typical methods is the competitive code method [26], which uses six directions of Gabor filters to filter a palmprint image. The direction of the Gabor filter that obtains the largest filtering response was extracted as the dominant direction of a palmprint. Similarly, the robust line orientation code (RLOC) method [27] designed twelve Radon-based filters to obtain the dominant directions of the palmprint. Extended from the competitive code method, the double-orientation coding method [28] extracted double direction features based on the top-two strongest line responses. In addition, the similar rule of winner-take-all is also used in the block dominant orientation code [29] , fusion code [30] and DRCC [31] methods.

Differently, multiple-direction-based methods propose to preserve the features on multiple directions. The representative multiple-direction-based methods include the orientation co-occurrence vector (BOCV) [33], extended BOCV (E-BOCV) [34], ordinal code [35], and neighboring direction indicator (NDI) [36] methods. For example, the BOCV method defined six Gabor filters to convolve with a palmprint image, and the results of the six filter responses were encoded. Extended from BOCV, E-BOCV extracted six direction code maps as the BOCV, and meanwhile filtered out the fragile direction points based on the magnitudes of filtering responses. In addition, the NDI method encoded the comparative response results between neighboring orientations among six orientations. Sun *et al.* [35] extracted three orthogonal direction codes by using three orthogonal Gaussian filters.

For the third category, a bank of templates are also used to convolve with palmprint to characterize the direction features, and then the statistics of one or multiple direction features are encoded. For example, the local line directional patterns (LLDP) method [37] encoded two direction features of a palmprint and formed the histogram-based direction descriptor. The LMDP method [38] calculated and concatenated the blockwise statistics of multiple dominant directions as the palmprint descriptor. Jia *et al.* [23] proposed a histogram of oriented line (HOL) method by calculating statistical energy on different orientations for palmprint recognition. Fei *et al.* [39] extracted the apparent direction features from the surface layer and the latent direction features from the energy map layer of a palmprint, and then a joint histogram is constructed as the final feature. In addition, Li *et al.* [40] extended the Local Tetra Pattern to Local Micro-structure Tetra Pattern (LMTrP) palmprint descriptor. Zhang *et al.* [17] used the blockwise histograms of the competitive code forming the feature vectors of a palmprint.

The direction-based palmprint recognition methods with promising accuracies have proved the success of the direction features for palmprint recognition [7]. Existing work generally extracted different kinds of direction features of a palmprint.

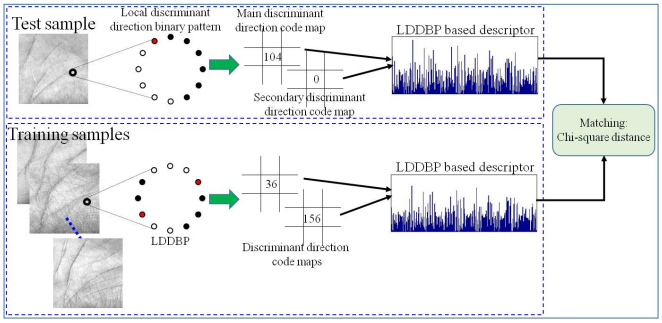

Fig. 1. The basic idea of the proposed method. For each palmprint image, local discriminant direction binary pattern are extracted, and then the most discriminant direction features are exploited. Further, the blockwise histograms are correspondingly computed and concatenated to form the LDDBP-based palmprint descriptor.

However, to the best of our knowledge, there is no work to investigate the essential discriminability of different directions. Therefore, the most discriminant direction representation is not yet exploited. To address this, in this article, we propose a novel model to characterize the discriminative power of different kinds of directions so that more discriminative direction features can be exploited. Then, we propose an effective and compact discriminant direction descriptor for palmprint recognition. Fig. 1 outlines the basic framework of the proposed method. Extensive experiments on different types of palmprint databases are conducted to show the effectiveness of the proposed method.

The main contributions of this paper can be summarized as follows:

- The connection between the direction feature extraction model and the discriminability of directions is established, and a novel exponential and Gaussian fusion model (EGM) is proposed to characterize the essential discriminability of different directions of palmprints. The EGM can better demonstrate the reasons why the state-of-the-art methods achieve promising performance. More importantly, the EGM provides us with an effective guideline for the potential discriminant direction selection for the optimal palmprint representation.
- We propose a local direction binary pattern (LDDBP) for the discriminant direction feature extraction. LDDBP can better describe the direction changes and implicitly denotes the multiple dominant direction features of a palmprint. Guided by the EGM, the top-three discriminant direction features are exploited from the LDDBP, and a compact LDDBP-based descriptor is designed for palmprint representation and recognition.
- Extensive experiments, as well as the comparison from the state-of-the-art deep-learning methods, on four widely used palmprint databases, are presented to demonstrate the effectiveness of the proposed method.

The remainder of this paper is organized as follows. Section II briefly review the related work. Section III proposes a local discriminant direction binary pattern for palmprint representation and recognition. Section IV conducts the experiments, and finally section V draws the conclusion of this paper.

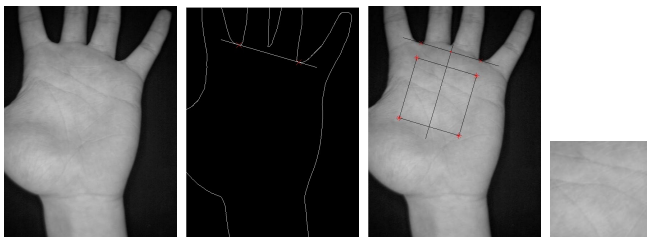

(a) (b) (c) (d)

Fig. 2. The basic procedure of the ROI extraction. (a) An input palmprint image. (b) The low-pass Gaussian filter is used to smooth the palmprint image, which is then converted into a binary image by thresholding, so as to obtain the boundaries of the binary image by using a boundary tracking algorithm. (c) The landmarks at the bottom of the gaps between fingers is used to establish a coordinate to determine the location of the ROI. (d) The sub-image located at a certain area of a palmprint is cropped and normalized to a fixed size, which is the ROI of the palmprint image.

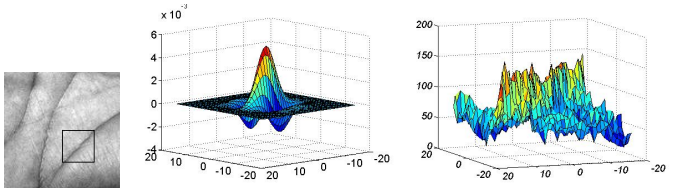

(a) (b) (c)

Fig. 3. The basic idea of direction feature extraction of a palmprint. (a) A palmprint image with a clearly visible line feature. (b) A Gabor template. (c) The upside-down intensity value map of the local patch of the palmprint.

II. Related Work

In this section, we briefly review the ROI extraction, the basic model of direction feature extraction, and direction feature representation of palmprint images.

A. ROI Extraction

In general, preprocessing is performed on a palmprint image to extract the region of interest (ROI) before feature extraction. The procedure of ROI extraction is depicted in Fig. 2. It is seen that the location of the ROI is essentially determined by the reference points, which are stably located at the bottom of gaps between the index and middle fingers and between the ring and little fingers. Therefore, the ROIs of palmprint images are generally aligned on both rotation and translation.

B. The Basic Rule of Direction Feature Extraction

In direction feature extraction of a palmprint, the common rule is to use line-structure detectors, such as Gabor filter, to characterize the direction feature of palmprint. To better illustrate the procedure of direction extraction, we take a palmprint image with a clearly visible line feature as an example, as shown in Fig. 3(a). Fig. 3 (b) depicts a Gabor filter with a "line-model" [26]. It is known that the black lines of the palmprint image usually have smaller gray values, and the line-model of the Gabor template has larger values. Thus, in real application, we usually subtract the gray values of a palmprint image with 255 to obtain the "upside-down" [26] palmprint image. Fig. 3 (c) shows the upside-down intensity value map of the local patch of Fig. 3 (a). It is not hard to deduce that the Gabor filter with the consistent direction with the line feature of the palmprint image can obtain a strong filtering response.

Inspired by this observation, the most dominant direction of palmprint can be detected by using a bank of filters with a series of pre-defined directions. Among them, one filter could generate the strongest filtering response with the palmprint, and the direction of which should be highly similar with the direction of the palmprint. Hence, the direction of the filter that maximizes the filtering response can be considered as the dominant direction feature of the palmprint. In general, the real part of Gabor filter is the most powerful tool for direction feature extraction, which has the following general function:

$$G(x, y, \theta, \mu, \sigma, \beta) = \frac{1}{2\pi\sigma^2} exp\{-\pi(\frac{x^2}{\sigma^2} + \frac{y^2}{\beta^2})\} \times cos(2\pi\mu(xcos\theta + ysin\theta)), \quad (1)$$

where μ is the radial frequency in radians per unit length, σ and β denote the standard deviations of the elliptical Gaussian along the x and y axis, respectively. The ranges of x and y control the sizes of the function. The optimal parameter setting can be referred to the study of [24]. θ defines the direction of the Gabor function. In practice, a bank of Gabor filters with directions of $\theta_j = (j-1)\pi/N_\theta$ is usually defined, where N_θ is used as the direction number of Gabor functions, and j is the corresponding direction index. To better characterize the direction of palmprint, in this paper N_θ is empirically set to 12. The convolution between the Gabor functions and palmprint image I is as follows:

$$r_j(x, y) = G(\theta_j) * (255 - I(x, y)), \quad (2)$$

where "*" denotes the convolution operator. A bank of Gabor functions with different directions can obtain a group of convolved results with the palmprint image. Among them, the Gabor function that produces the maximum convolved result is selected, and the direction of which is treated as the most dominant direction of the palmprint:

$$\theta(I(x, y)) = arg \max_{\theta_j} r_j(x, y). \quad (3)$$

C. Direction Feature Representation

Direction features of palmprint images are usually represented by pixel-wise codes, which are also matched in pixel-wise level in palmprint recognition [26], [33]. However, it is inevitable that palmprint images have misalignments due to the image capture device and the external environment, especially for contactless palmprint images. The pixel-wise direction feature codes are sensitive to small amount of registration errors between the probe and gallery samples [17]. To this end, the blockwise statistics, such as histograms, of direction features are usually used as palmprint descriptor due to its promising robustness to small misalignments.

The local direction based descriptor is originally designed focusing on the images with rich edge features. For example, local direction pattern (LDP) [41] calculated the edge

responses by convolving Kirsch edge masks of a point with the eight neighbors. Then, the top-k edge responses were selected and binarized to construct the LDP codes, and the blockwise histograms of which were calculated. After that, the enhanced local directional pattern (ELDP) [42] and local directional number (LDN) [43] encoded two selected direction features forming the blockwise direction histogram descriptor. Inspired by that, Luo *et al.* [37] proposed a local line directional pattern (LLDP) for palmprint representation. It used both the MFRAT and Gabor filters with twelve directions to obtain the line responses of a palmprint, and then the similar schemes as ELDP and LDN were used to encode two specific directions. Lastly, the blockwise histograms of the direction codes were computed and concatenated as the palmprint feature. Quite recently, the blockwise statistics of direction feature codes have been widely used as the feature representation of palmprint images [17], [38]–[40].

III. Discriminant Direction Feature Extraction

In this section, a Gaussian-like model is proposed to demonstrate the discriminability of different directions. Further, a local discriminant direction binary pattern is proposed for the discriminant direction feature extraction. Finally, the LDDBP-based palmprint descriptor is formed for palmprint recognition.

A. The Discriminability of Direction Features

It is seen that both the dominant and other direction features are widely used for palmprint recognition. However, to the best of our knowledge, there is no work to investigate and analyze the discriminative power of different direction features. Motivated by this, in this section, we aim to investigate the essential difference of the direction features.

Based on the rule of direction feature extraction, the line-like templates with pre-defined directions are generally used, and the convolved results between the templates and palmprint image are the basis of direction feature extraction. For instance, some methods extract the direction features based on the maximum convolved values [26], [30], and some other methods extract the direction features based on both the maximal and minimal the convolved results [44]. Therefore, we believe that the discriminability of the direction features is heavily related with the convolved results between the templates and a palmprint. In addition, a palmprint image generally contains two kinds of points, namely, the points with visible lines such as the principal lines and the points with invisible line. In the following, we discuss the discriminability of the direction features for both kinds of the points based on the convolved results between the templates and the points.

To better illustrate the direction feature extraction for a point with a obviously dominant direction, we take a palmprint image with a clearly visible line feature as an example, as shown in Fig. 4 (a). We use twelve Gabor filters with directions of $(j-1)\pi/12(j=1,2,\ldots,12)$ to convolve the point on the visible line obtaining twelve filtering responses, as shown in Fig. 4 (b). The Gabor filter with the direction of $\pi/4$ produces the strongest filtering response (maximum convolved result) among all twelve templates. Therefore, according to the competitive code method, we take the $\pi/4$ as the dominant direction feature of the point in the palmprint image, which is technologically sound. In general, a Gabor filter has an obvious line-model [26], as an example shown in Fig. 4 (c). The filtering response between a Gabor filter and the point is essentially the sum of the pixel values weighted by the Gabor filter of a local patch. Theoretically, when a Gabor filter has a similar direction as the palmprint line, the line-model of the Gabor filter will better overlap the palmprint line, as shown in Fig. 4 (d), resulting to a stronger filtering response with the palmprint line. In other words, the filtering response between a Gabor filter and a point in a palmprint line is theoretically proportional to the overlapped area of line-models between the filter and the palmprint line. We abstract the convolution in Fig. 4 (d) as Fig. 4 (e). It clearly shows that the line-model of the Gabor filter has a larger overlapped area with the palmprint line if they have more similar directions, producing a larger filtering response. Therefore, the filtering response between a Gabor filter and a palmprint line is essentially related to its direction difference, which can be defined as: $|\theta_{Gabor}+\pi-\theta_{line}|\ mod\ \pi$, where θ_{Gabor} and θ_{line} represents the direction angles of the line-models of the Gabor filter and the palmprint line, respectively. In the following, we further discuss the relationship between the filtering response and the direction difference between a Gabor template and a palmprint line.

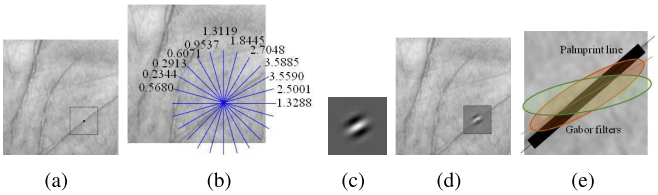

Fig. 4. An illustration dominant direction extraction of a point within a local patch of a palmprint image with a visible line feature. (a) A palmprint image with a visible line direction feature. (b) The convolved results between Gabor filters and a point of the palmprint image on twelve directions. (c) A Gabor filter. (d) The convolution of the Gabor filter and a point within a local patch with a line feature. (e) The convolution procedure model between the filters and a palmprint line.

We assume that a Gabor filter has the same direction as the palmprint line. The convolution result, as well as the overlapped area between the line-models of the filter and the palmprint line, should be larger than that of other directions. Now, if we change the direction difference to $\Delta\theta$, as shown in Fig. 5 (a, blue arrow), the overlapped area between the line-models of a Gabor filter and the palmprint line will be reduced, as shown in Fig. 5 (a, from green area to blue area). Then, if we further change the direction difference with the same $\Delta\theta$, as shown in Fig. 5 (a, purple arrow), the overlapped area changes by an even smaller amount than the former one, as shown in Fig. 5 (a, from blue area to purple area), due to the elliptical shapes of the Gabor filters. Therefore, we can deduce that, starting from the direction difference of 0, as the direction difference is gradually increasing, the corresponding overlapped area and the filtering response (convolved result) will be reduced rapidly at the beginning and then slowly afterwards. The convolved result reaches its minimum value

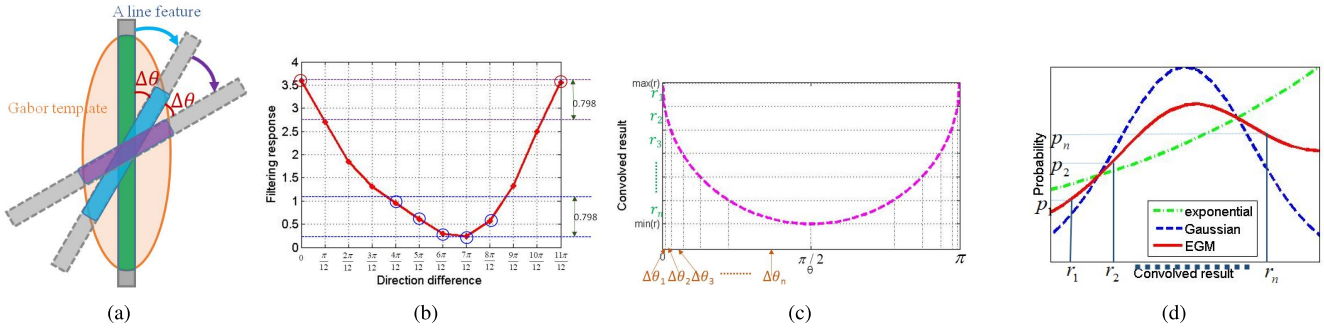

Fig. 5. The relationship between the discriminability of direction features and direction feature extraction model. (a) A convolution operation model. (b) The convolved result distribution of an example. (c) The convolved result distribution model; and (d) The curve of the EGM.

when the direction difference is about $\pi/2$, that is, the Gabor filter and the palmprint line have perpendicular directions. As the direction difference further gradually increases, the convolved result will increase slowly at the beginning and then increase rapidly. It reaches the maximum value again when the direction difference reaches π (the same as the direction difference of 0). We also take the convolution of Fig. 4 (b) as an example. The filtering responses between the Gabor filters and the palmprint line along the direction difference can be depicted as Fig. 5 (b). It shows that the filtering response reaches its maximum value when the direction difference is 0. When the direction difference changes from 0 to $\pi/12$, the corresponding filtering response is reducing more faster than that from $6\pi/12$ to $7\pi/12$. Therefore, the relationship between the direction difference and the convolved result can be modeled as shown in Fig. 5 (c), where the $x\text{-}axis$ represents the direction difference and the $y\text{-}axis$ denotes the corresponding convolved results.

Fig. 5 (b) shows that few Gabor filters can produces larger filtering responses. For example, only two Gabor filters with two direction differences of 0 and $11\pi/12$ can produce larger filtering responses (convolved results), as shown in Fig. 5 (b, purple circles). By contrast, five Gabor filters can produce smaller filtering responses, as shown in Fig. 5 (b, blue circles). Hence, if the directions of the Gabor filters corresponding to the top-two filtering responses are selected as the direction features of a palmprint, the directions of the filters with direction differences of 0 and $11\pi/12$ can be easily extracted. Because very few Gabor filters can produce as large a filtering response as them. If the directions of the Gabor filters producing the smallest two filtering responses are taken as the direction features of a palmprint, the directions of the filters with direction differences of $6\pi/12$ and $7\pi/12$ can be extracted in this example. However, these directions could be easily affected by small rotation or noise because many Gabor filters can produce very close filtering responses to them. Therefore, the direction features corresponding to larger convolved results should be more stable than that of the smaller convolved results, and thereby achieve a better performance at palmprint representation.

Fig. 5 (c) also shows that, with a certain range of the convolved results (e.g., r_i), a larger convolved result value (e.g., r_1) corresponds to a smaller range of the direction difference (e.g., $\Delta\theta_1$). This means that fewer directions of the templates can obtain the large convolved results. Comparatively, a smaller convolved result (e.g., r_n) corresponds to a larger range of the direction difference (e.g., $\Delta\theta_n$), which means that more directions of the templates can obtain these smaller convolved results. In other words, suppose there have many Gabor filters with various and evenly distributed directions, a stronger filtering response can be produced by a few Gabor filters and a smaller filtering response can be easily obtained by more Gabor filters. Thus, the probability of producing a larger filtering response is smaller than that of producing a smaller one. We believe that the directions of the Gabor filters producing larger filtering responses are more stable than that of producing smaller responses, and thus achieve a better performance for palmprint recognition. Therefore, we think that the direction of the Gabor filter that produces a stronger filtering response have higher discriminability.

It is also seen that a palmprint usually contains many points without clearly visible line features. For those points, in direction feature extraction, it is believed that very few templates can obtain the maximum filtering response, and very few templates can reach the minimum filtering response. Comparatively, a medium convolved result can be obtained by more templates with more directions. Thereby, we assume that the probability of the convolution results between the templates and these points satisfy a Gaussian model, as shown in Fig. 5 (d, blue line). In addition, we assume that the probability of the convolution results between the Gabor filters and the palmprint points with visible lines follows an exponential-like model, as shown in Fig. 5 (d, green line). A palmprint generally contains different kinds of points with visible, invisible or medium-visible dominant direction features. Therefore, we can reasonably assume that the possibility of the convolved result between a template and palmprint follows an exponential and Gaussian fusion model (EGM), which can be represented as follows:

$$p_{c\_r} \sim \lambda_1 e^{k*c\_r} + \lambda_2 Gaus(\mu, \sigma^2), \tag{4}$$

where c_r represents the convolved result, and $Gaus$ represents a Gaussian function. λ_1, λ_2, k, μ and σ are the parameters. Of them, the balance parameter, that is, λ_1 and λ_2, can be set according the characteristics of palmprint. For instance, λ_1 should be larger than λ_2 if a palmprint contains

a large number of line features, and otherwise λ_2 should be larger than λ_1. In Fig. 5 (d), the red line shows an example of the EGM, where the $x-axis$ denotes the filtering responses (i.e., convolved results) between the templates and the points in a palmprint image, and the $y-axis$ represents the corresponding probabilities of the convolved results. For the sake of clarity, the value of $x-axis$ is gradually decreasing, i.e., $r_i > r_{i+1}$.

From the curve of the EGM, as shown in Fig. 5 (d, red line), we can obtain the following findings: (1) the direction of the Gabor filter that produce the strongest filtering response generally has the best discriminability; (2) the discriminability of the direction features will decrease as the filtering response decreases, and then it will increase as the filtering response further decreases; (3) the direction of the Gabor filter that produces the smallest filtering response usually have a relatively higher discriminability.

The EGM generally represents the probability distributions of the convolved results between the filters and the palmprint. More importantly, the model essentially reflects the discriminability of different direction features. The EGM shows that the most dominant direction generally has the best discriminability. This validates the effectiveness of the winner-take-all based methods that extract the most dominant direction feature of a palmprint, such as the competitive code and RLOC methods. Further, the directions of the templates producing the maximum and minimum filtering responses usually have higher discriminability than the neighboring directions of them. This is the reason why the dual competitive code method [44] extracted the direction features based on both the maximal and minimal Gabor filtering responses. In addition, the EGM shows that the direction feature with a larger line response behind the largest one possibly has higher discriminability. This finding is consistent with the results of the DOC and LLDP methods. Therefore, the proposed model can better demonstrate the reasons why conventional methods can achieve promising performance. Furthermore, the model provides us with an effective guideline to exploit the most discriminant directions for the optimal palmprint feature representation.

B. Local Discriminant Direction Binary Pattern

The conventional winner-take-all rule can only extract the single-dominant direction of a palmprint. However, a palmprint usually contains a number of crossing and fold lines, which lead to multiple-dominant directions in a palmprint. To this end, we introduce an effective scheme to represent the multiple-dominant direction cases of a palmprint.

It is noted that the convolved result between a filter and a palmprint line is generally proportional to the overlapping area between the line-models of the filter and the palmprint line. Based on the observation, it can be deduced that a filter with a more closer direction to the line direction can produce a larger overlapped area with the line, thus generating a larger convolved result. A simple and effective way to represent the relationships between two filtering responses along neighboring directions can be written

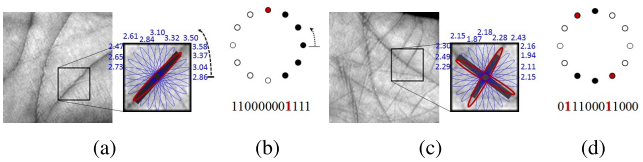

Fig. 6. The basic idea of the LDDBP. (a) The convolved results of a point with a visible line direction feature. (b) The LDDBP with a dominant direction corresponding to panel a. Specially, the above circles demonstrate the circular property of the LDDBP, where the black and white circles correspond to 1 and 0, respectively. The below binary string is the LDDBP. The arrow denotes the starting direction and red represents the exact dominant direction. (c) A point with double dominant directions. (d) The LDDBP with double dominant directions corresponding to panel c.

as follows:

$$S = [s(r_{N_\theta} - r_{N_\theta - 1}), \ldots, s(r_j - r_{j-1}), \ldots, s(r_2 - r_1), s(r_1 - r_{N_\theta})], \quad (5)$$

where r_j represents the convolved result on the jth direction, $s(x)$ equals to 1 if $x > 0$ and 0 otherwise, and N_θ is defined in Section II. In other words, it is represented as "1" if the convolved result along a direction is larger than that along the adjacent clockwise direction, and otherwise it is marked as "0". By assigning a binomial factor 2^j for each element $s(r_j - r_{j-1})$ in S [45], it can be transformed into a uniform binary pattern, which is named the local discriminant direction binary pattern (LDDBP), as follows:

$$LDDBP = \sum_{j=1}^{N_\theta} s(r_j - r_{\varphi(j)}) 2^j, \quad (6)$$

where $\varphi(j)$ denotes the adjacent clockwise direction index of j. It is noted that LDDBP is circular and the direction indices of 1 and N_θ are adjacent. That is, $\varphi(j)$ equals to N_θ if $j = 1$ and $(j-1)$ otherwise, and it can be directly calculated as follows:

$$\varphi(j) = mod(j - 2, N_\theta) + 1, \quad (7)$$

where mod denotes the Mudulo operator.

The LDDBP can effectively reflect the multiple dominant directions of a palmprint. Specifically, the "01" in the LDDBP essentially denotes a dominant direction, where "1" means that the convolved result along the current direction is larger than that along the clockwise neighbor direction, and "0" denotes that it is smaller than that on the counterclockwise neighbor direction. The number of "01" in an LDDBP denotes the number of dominant directions of a point. Further, in a "01" sequence, the position of the "1" exactly represents the index of the dominant direction. Fig. 6 shows the basic idea of the LDDBP. The LDDBP of Fig. 6 (b), i.e., "110000001111", represents that it contains only one dominant direction at $3\pi/12$. The LDDBP of "011100011000" in Fig.6 (d) denotes that the current point has two dominant directions, i.e., $4\pi/12$ and $10\pi/12$. Therefore, the LDDBP can not only describe how the direction feature changes and but also implicitly denotes the multiple dominant direction features of a palmprint point, including the number of the dominant directions and their exact positions.

The dominant direction number (DDN) is essentially determined by the "01" in an LDDBP. It is easy to check that there is a one-to-one correspondence between sequence pairs of "01" and "10" in an LDDBP. Therefore, the DDN can be calculated as follows:

$$DDN_{LDDBP} = \frac{1}{2}\sum_{j=1}^{N_\theta} |s(r_j - r_{\varphi(j)}) - s(r_{\varphi(j)} - r_{\varphi(\varphi(j))})|. \tag{8}$$

The dominant direction index (DDI), which is the position of "1" in a "01" of an LDDBP, directly denotes the index of a dominant direction. The DDI of an LDDBP can be obtained as follows:

$$DDI_{LDDBP} = \{j | s(r_j - r_{\varphi(j)}) - s(r_{\phi(j)} - r_j) = 1\}, \tag{9}$$

where $\phi(j)$ denotes the adjacent counterclockwise direction index of j, which equals to 1 if $j = N_\theta$ and $j+1$ otherwise. $\phi(j)$ can be simply obtained by the following:

$$\phi(j) = mod(j, N_\theta) + 1. \tag{10}$$

The numerical results in the study of [38] show that a plenty of points in a palmprint have multiple dominant direction features (DDF). Actually, an LDDBP with double dominant direction features can be divided into two sub-LDDBPs, and each sub-LDDBP contains only one dominant direction feature. Specifically, an LDDBP with double DDFs generally contains two "01" and two corresponding "10" sequences. We divide the "...10..." sequences in an LDDBP into "...1" and "0..." to generate two sub-LDDBPs with the general form of "0...01...1," which is named as a basic LDDBP. For example, "0111<u>00011</u>000" can be divided into "****00011***" and "0111*****000." Therefore, each sub-LDDBP can be considered to contain only one "01" and one "10." An LDDBP with more than two DDFs can also be divided into multiple sub-LDDBPs, each of which contains one "01" and one "10." Theoretically, the EGM is effective for each sub-LDDBP and also a normal LDDBP.

C. LDDBP-Based Palmprint Representation

The EGM effectively demonstrates the discriminative power of the different direction features of a palmprint. Guided by the EGM, we see that the directions corresponding to both the maximum and minimum convolved results usually have the best discriminability. In addition, the directions producing a stronger filtering response behind the strongest response should also carry higher discriminability. To balance the discriminability and the feature size of direction features, in this paper, the directions corresponding to the maximum, the second maximum and the minimum convolved results are selected as the top-three discriminant direction features, forming the palmprint descriptor. To simplify, the direction feature corresponding to the kth maximum filtering response is referred to as the kth dominant direction.

To effectively represent the selected discriminant direction features, we first select the principal LDDBP of the points in a palmprint. The LDDBP with only one dominant direction feature is directly the main LDDBP (LDDBP$_m$). For the points with double dominant direction features corresponding to double sub-LDDBPs, we select the sub-LDDBP having the DDF with the maximum filtering responses as the LDDBP$_m$, and another one is considered as the secondary LDDBP (LDDBP$_s$). Therefore, only the LDDBP with two or more DDFs has the LDDBP$_s$. Because very few points of a palmprint have more than two DDFs, we only use the LDDBP$_m$ and LDDBP$_s$ to represent a palmprint. In the following, we use a compact scheme to label the LDDBP$_m$ and the LDDBP$_s$.

In a basic LDDBP containing only one "01" pattern, the second dominant direction feature is always adjacent to the first dominant direction. Therefore, the first and second dominant directions can be effectively labeled as: $2\times D - s(r_{\varphi(j)} - r_{\phi(j)})$, where D denotes the first dominant direction index in the basic LDDBP. It is not hard to check that the label range is from 1 to $2N_\theta$. By contrast, the conventional methods, such as LLDP method, uses N_θ^2 codes to represent the first and second dominant direction features. Therefore, the proposed label scheme seems to be more effective than the conventional methods.

To further compact the representation codes, we use the direction distance to combine the last dominant direction with the top-two dominant direction features. Particularly, the LDDBP$_m$ is labeled as follows:

$$\begin{aligned} L_m = (2\times D_m - s(r_{\varphi(D_m)} - r_{\phi(D_m)}) - 1)\times(N_\theta - 1) \\ + mod(D_m - D'_m + N_\theta, N_\theta), \end{aligned} \tag{11}$$

where D_m and D'_m are respectively the first and last dominant direction indices with the maximum and minimum filtering responses in the LDDBP$_m$. Similarly, the LDDBP$_s$ can be represented as:

$$L_s = \begin{cases} 0 & \text{if DDN} = 1 \\ (2\times D_s - s(r_{\varphi(D_s)} - r_{\phi(D_s)}) - 1) & \\ \times(N_\theta - 1) + mod(D_s - D'_s + N_\theta, N_\theta) & \text{if DDN} \geq 2, \end{cases} \tag{12}$$

where D_s and D'_s denote the direction indices corresponding to the largest and smallest filtering responses, respectively, in the LDDBP$_s$. L_m and L_s are considered as the main and secondary discriminant direction codes of a palmprint, respectively. For a point of a palmprint image, the lengths of both L_m and L_s are $2N_\theta(N_\theta - 1)$.

It is seen that different areas of a palmprint have different textural and line characteristics. To better represent the position-specific features and overcome the slight misalignment of palmprint images, we use the blockwise-based statistics to represent the palmprint images. Specifically, a palmprint image is uniformly divided into a set of nonoverlapping local patches. Then, we calculate the LDDBP map, including both the LDDBP$_m$ and LDDBP$_s$ maps, for each block. Third, we compute the blockwise histograms of L_m and L_s for each block, and further concatenate them to form the L_m and L_s-based descriptors of the palmprint, respectively. It is pointed out that $L_s = 0$ means that an LDDBP has non LDDBP$_s$. Therefore, we only count $L_s \geq 1$ in the L_s histogram calculation. Finally, we concatenate both the

L_m- and L_s-based descriptors together to form the LDDBP-based descriptor.

D. LDDBP-Based Palmprint Recognition

In palmprint matching, the LDDBP-based descriptors of palmprint images are first calculated. After that, the simple and effective Chi-square distance is used to measure the similarity between the two LDDBP descriptors. Suppose the two LDDBP descriptors of two palmprint images are P and Q, respectively, their Chi-square distance is:

$$\chi^2(P, Q) = \sum_{i=1}^{N_H} \frac{(p_i - q_i)^2}{p_i + q_i}, \tag{13}$$

where p_i (q_i) is the value of P (Q) at the ith bin, and N_H is the length of the LDDBP descriptor. In summary, the similarity of two palmprint images can be evaluated by calculating the Chi-square distance between the LDDBP descriptors of them. A small Chi-square distance means a high similarity between the two compared palmprint images.

IV. Experiments

In this section, to evaluate the effectiveness of the proposed method, we conducted a number of experiments on four publicly and widely used palmprint databases, including the PolyU, IITD, GPDS and CASIA palmprint databases.

A. Palmprint Databases

The PolyU palmprint database [46] contains 7,752 palmprint images collected from 386 palms of 193 individuals. The images were captured in two sessions with an interval of around 60 days. An individual was asked to provide about 10 samples for both the left and right palms. Actually, some palms, such as the 137th palm, provided more than 17 images in the first session, and some other palms, such as the 150th palm, provided only one image in the second session. As a result, a palm in the PolyU database might have about 11 to 27 samples. The ROI images with the sizes of 128×128 pixels have also been included in the database.

The IITD palmprint database [47] consists of 2,601 contactless palmprint images collected from 460 palms corresponding to 230 subjects with both the left and right palms. Five to six samples were captured for each palm. Specially, the left palm of the eighth subject provided 7 palmprint images. The IITD palmprint database has provided the corresponding ROIs with the sizes of 150×150 pixels.

The GPDS palmprint database [48] includes 1,000 contactless palmprint images collected from the right palm of 100 volunteers, each of which provided 10 palmprint images. The GPDS database provides both the original palmprint images and the corresponding ROIs. In our experiments, the ROIs are resized to 128×128 pixels.

The CASIA palmprint database [49] contains 5,502 palmprint images collected from 312 subjects. About 8 to 10 palmprint images were respectively captured from the left and right palms. It is noted that the 75th and 167th subjects provided no palmprint image, and the last right palmprint image of the 270th individual does not belong to the subject. As a consequence, the used CASIA database actually includes 5,501 palmprint images from 310 subjects with 620 palms. In the experiments, the preprocessed method in [24] is used to crop the palmprint ROIs with sizes of 128×128 pixels in the CASIA database.

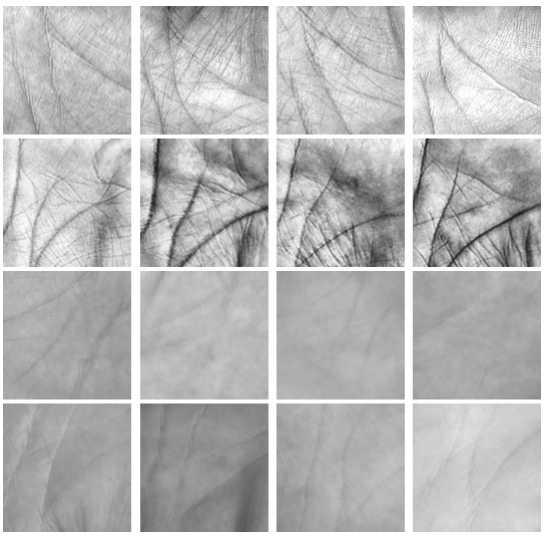

Fig. 7. Some typical palmprint ROI images. The palmprint images of the first to fourth lines are selected from the PolyU, IITD, GPDS and CASIA databases, respectively.

The PolyU palmprint images were captured under a contact-based device which used the user-pegs to restrict the placement of palms. By contrast, the palmprint images from the other three databases, including the IITD, GPDS, and CASIA databases, were captured under unconstraint environment. Therefore, palmprint images in the IITD, GPDS and CASIA databases were possibly variant on postures, positions, scales, and illumination. Fig. 7 shows some typical sample images selected from the PolyU, IITD, GPDS and CASIA databases, respectively.

B. Palmprint Identification

Palmprint identification is a one-against-many matching process to determine the class label of a query palmprint image. In general, a set of palmprint images with known class labels is selected as the training sample. A query sample will be compared with the training sample. The class label of the training sample that has the maximum similarity with the query sample is treated as the class label of the query sample.

In the following identification experiment, for a database, we randomly selected n palmprint images per palm to form the training set, and used the rest for testing, where n is set from 1 to 4. The class label of the training sample that produces the maximum matching score, which is the smallest Chi-square distance in the proposed method, is assigned to the query sample. We also test the conventional powerful direction-based methods and compare them with the proposed method. The compared methods include the competitive code [26], ordinal code [35], E-BOCV [34], neighboring direction indicator (NDI) [36], LLDP [37], ALDC [39], CR_CompCode [17],

TABLE I

THE IDENTIFICATION ACCURACY (%) (AVERAGE ACCURACIES ± STANDARD DEVIATIONS) OBTAINED BASED ON DIFFERENT METHODS ON THE POLYU, IITD, GPDS AND CASIA PALMPRINT DATABASES

	Competitive	Ordinal	E-BOCV	NDI	LLDP	ALDC	CR_CompCode	E-SRC	HOL	AlexNet	VGG-16	ResNet-50	LDDBP
PolyU	95.32±0.38	94.31±0.53	92.20±0.60	96.43±1.08	99.33±0.13	99.35±0.08	96.77±0.84	96.55±1.34	98.71±0.77	62.15±0.81	57.25±4.08	58.79±3.90	**99.65±0.10**
	97.48±0.40	97.31±0.73	95.29±1.85	98.66±0.64	99.54±0.30	99.63±0.20	99.15±0.61	97.61±0.59	99.61±0.16	85.02±1.18	86.54±1.80	82.79±2.17	**99.83±0.14**
	98.08±0.85	97.72±0.90	95.38±0.42	99.11±0.47	99.70±0.17	**99.85±0.12**	99.33±0.43	99.08±0.27	99.77±0.15	93.05±0.62	92.52±0.66	92.90±1.12	99.79±0.03
	98.83±0.66	98.33±0.91	97.66±1.86	99.29±0.45	99.83±0.13	99.80±0.14	99.38±0.23	99.25±0.50	99.78±0.11	97.24±0.44	97.06±1.09	97.51±0.62	**99.85±0.11**
IITD	45.92±2.60	42.25±2.01	60.73±1.04	49.83±1.09	84.03±0.58	85.07±0.10	78.14±1.32	62.38±2.19	84.88±0.90	46.36±2.11	56.62±3.47	56.24±6.14	**90.29±0.79**
	65.16±1.55	58.77±2.21	74.31±2.28	67.67±2.05	93.04±1.01	93.54±1.02	91.43±0.98	75.07±1.69	93.19±0.20	66.65±2.21	83.92±1.83	84.81±4.46	**95.55±0.43**
	72.25±2.40	70.73±1.47	84.10±1.24	77.99±0.78	95.08±0.61	96.15±0.91	93.69±1.21	79.12±1.69	95.12±0.47	83.12±1.37	88.21±2.26	94.18±1.59	**97.26±0.52**
	79.79±1.45	76.43±2.06	87.96±0.18	82.21±1.65	96.13±0.76	97.00±0.28	95.80±0.83	81.37±1.67	96.80±0.44	88.13±1.87	92.26±2.11	96.71±1.22	**97.81±0.89**
GPDS	61.73±2.62	56.18±9.63	60.56±7.89	68.51±2.85	82.29±1.50	85.53±1.82	81.78±2.15	68.21±2.26	79.35±4.47	62.28±3.86	64.32±2.67	62.97±2.26	**88.11±0.86**
	75.88±2.34	74.68±0.67	75.60±1.83	77.93±2.54	91.67±0.84	92.85±1.09	89.13±1.18	75.56±1.68	91.37±0.95	80.59±2.55	80.34±3.11	83.75±2.65	**95.03±1.13**
	80.03±3.93	82.17±1.30	84.71±1.25	86.40±2.92	94.05±1.11	95.06±0.93	91.71±1.32	85.10±1.67	93.31±0.90	86.14±1.68	87.86±2.06	91.34±1.66	**96.48±1.65**
	86.03±2.47	85.53±1.94	87.16±1.73	88.80±2.07	95.96±0.82	97.70±0.52	93.17±0.91	89.24±1.44	96.10±1.05	91.48±1.25	92.53±1.31	94.06±1.90	**97.70±0.48**
CASIA	55.21±0.61	47.26±7.12	60.50±6.18	55.75±0.69	82.62±2.90	86.16±1.03	79.90±1.92	68.51±4.90	83.03±0.47	71.78±1.75	71.28±2.24	85.89±2.17	**87.94±3.29**
	66.49±6.69	63.66±1.38	75.55±4.83	71.14±2.94	90.87±1.03	92.03±0.97	85.54±1.56	81.31±4.46	88.37±2.44	85.97±1.05	88.77±1.03	94.17±0.98	**94.68±1.49**
	79.45±1.44	73.26±2.03	82.83±1.35	76.94±4.87	93.31±1.05	93.65±2.18	88.05±1.90	85.77±5.40	92.45±2.88	92.24±0.73	92.61±0.82	**96.85±0.25**	95.44±1.04
	79.27±5.45	75.92±1.64	84.06±2.46	78.22±3.33	94.58±0.46	94.64±1.35	92.59±1.07	88.36±6.03	94.87±0.36	94.53±0.60	95.43±0.52	95.87±1.37	**97.27±0.12**

Ensemble-SRC (E-SRC) [19] and HOL [23] methods. For the sake of a fair comparison, in the experiments, the local block sizes of all the related methods are set as 16×16 pixels, unless otherwise stated. All the methods are repeated 10 times and the rank-one identification accuracies (average accuracies ± standard deviations) are reported.

Moreover, we implement three typical deep-learning models for palmprint recognition, including the AlexNet [50], VGG-16 [51] and ResNet-50 [52] models. AlexNet consists of eight learned layers, five convolutional layers and three fully connected ones. A 1000-way softmax connected with the last fully connected layer produces the classification results. Generally, VGG-16 has similar input and fully connected layers as the AlexNet. The main difference between the VGG-16 and AlexNet is in the hidden layers where the VGG-16 has a total of 5 pooling layers and 13 convolutional layers with small filter sizes of 3×3. All the hidden layers are equipped with ReLU nonlinearity. Comparatively, ResNet-50 has a similar architecture as the conventional networks except that it adds a shortcut connection to each of the 3 layers of the 3×3 filters, and it has 50 layers. The three CNN models are pretrained on the ImageNet database. Then, we further train each model with fine-turning based on 10 different gallery sets of a palmprint database so that 40 trained models are obtained for the four palmprint databases. It is pointed out that all the input palmprint ROI images are resized to 256×256 pixels, and the RGB channels are normalized with the same gray values of the samples. After that, we use each model to perform palmprint identification to obtain the average accuracies and corresponding standard deviations.

The comparative results of palmprint identification on the PolyU, IITD, GPDS and CASIA palmprint databases are summarized in Table I. It can be seen that the proposed LDDBP method generally outperforms the twelve compared methods including the popular deep-learning methods. In the cases of selecting one to four images for a palm as the training samples, the proposed method can increase approximately 12.37%, 4.94%, 2.58% and 1.18%, respectively, in the accuracies over the average accuracies of the twelve compared methods on the PolyU databases. As for the IITD database, the proposed method can respectively achieve approximately 27.58% 16.59%, 11.45% and 8.59% higher accuracies than the average accuracies of the twelve compared methods. In addition, the average accuracy improvements of the proposed method are approximately 18.63%, 12.42%, 8.32% and 6.00% on the GPDS database, and about 17.28%, 12.69%, 8.15% and 7.99% on the CASIA database, respectively. In particular, in the case of selecting one sample per each palm as the training sample, the proposed method improves by approximately 0.30% over the best of the twelve compared methods on the PolyU database. This improvement does not seem significant due to the fact that the samples of the PolyU database are captured using a contact-based methodology. Most methods can achieve high accuracies of over 99%. Comparatively, the proposed method improves around 5.41%, 5.82% and 2.05% over the best results of the twelve compared methods on the IITD, GPDS and CASIA databases, respectively, showing the competitive performance of the proposed method.

C. Palmprint Verification

Palmprint verification is a one-to-one palmprint matching procedure. A matching is labeled as a "genuine match" if both compared palmprint images are from the same palm, and otherwise the comparison is named as an "impostor match". In the verification experiment of this study, each palmprint image in a database is compared with all other samples with the same database by using the proposed method to compute the incorrect genuine matches and incorrect impostor matches. After that, the false acceptance rate (FAR), the false rejection rate (FRR) and the receiver operating characteristic (ROC) curve are calculated to estimate the performance of the proposed method. Further, we implement the representative direction-based palmprint recognition methods, including the competitive code, NDI, E-BOCV, LLDP, and HOL methods, and compare them with the proposed method. The ROC (FAR vs FRR) curves of different methods are depicted in Fig. 8. It can be seen that the proposed LDDBP method consistently achieves a lower FRR than the five compared methods against the same FAR, and it also obtains the lowest equal error rate (EER).

D. Palmprint Identification on the Noisy Palmprint Datasets

In practical applications, palmprint images are usually suffer some noise due to the capture environment and

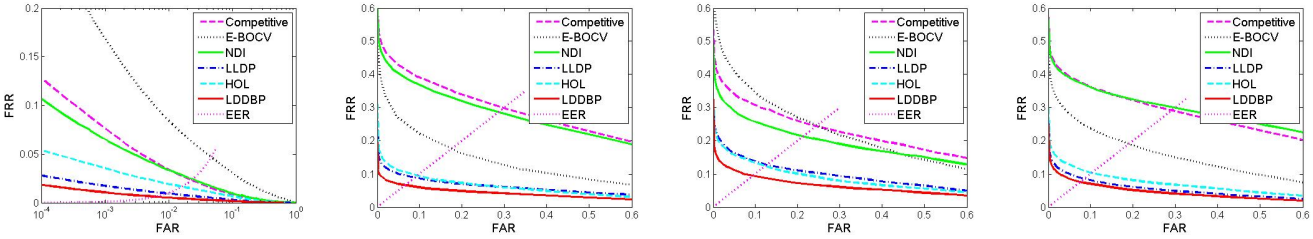

Fig. 8. The ROC curves of different methods on the (a)-(d) PolyU, IITD, GPDS, and CASIA databases.

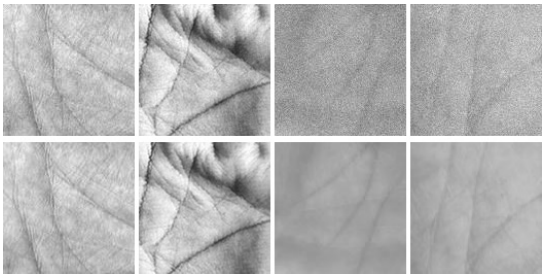

Fig. 9. The noisy palmprint image samples. The first line shows four noisy palmprint image samples and the second line shows the corresponding original palmprint images selected from the PolyU, IITD, GPDS and CASIA databases, respectively.

image processing. To simulate the noisy palmprint images, we add different levels of Gaussian noise on the samples of the PolyU, IITD, GPDS and CASIA databases. Specifically, we add Gaussian noise with a mean of 0 and variance of 5 on the palmprint image samples of the PolyU and IITD databases, and with a mean of 0 and variance of 10 on the samples of the GPDS and CASIA databases, respectively, to form four noisy palmprint datasets. Fig. 9 shows some noisy palmprint image samples selected from the four synthetic datasets.

Based on the four synthetic palmprint image datasets, we conduct palmprint identification to test the performance of the proposed method and compare it with the representative direction-based palmprint recognition methods. In this study, we mainly implement the four recently representative palmprint recognition methods achieving the competitive performance, including the E-BOCV, LLDP, CR_CompCode and HOL methods. Given a dataset, we randomly select n ($n = 1, 2, 3, 4$) images from each palm as the training samples and the remaining as the query samples. We run all the methods 10 times and summarize the identification results (average accuracies $\pm$ standard deviations) in Table II.

It can be seen from the table that the performance drops of all the methods are small on the noisy PolyU and IITD datasets when compared with the results on the original palmprint databases in Table I. The main reason is that the added Gaussian noise on the PolyU and IITD databases is small-level, which does not heavily affect the quality of the palmprint images. By contrast, the added high-level of Gaussian noise seriously affect the quality of the palmprint images on the GPDS and CASIA databases resulting to the significant accuracy drops of all the methods on palmprint identification. Therefore, the proposed method as well as the conventional direction-based

TABLE II

THE RANK-ONE IDENTIFICATION ACCURACY (%) OBTAINED BY DIFFERENT METHODS ON THE NOISY POLYU, IITD, GPDS AND CASIA PALMPRINT DATABASES

	E-BOCV	LLDP	CR_CompCode	HOL	LDDBP
PolyU	91.79±0.94	99.03±0.23	96.54±0.01	98.58±0.60	**99.50±0.14**
	95.47±1.83	99.42±0.14	98.93±0.30	99.54±0.21	**99.75±0.06**
	95.50±1.40	99.67±0.13	99.36±0.32	99.61±0.06	**99.80±0.12**
	97.36±1.55	99.78±0.09	99.41±0.01	99.76±0.19	**99.81±0.08**
IITD	60.33±0.87	83.06±0.83	78.63±0.54	83.62±0.81	**89.66±0.62**
	73.47±2.86	93.00±0.62	90.52±0.80	91.93±1.55	**95.37±0.33**
	83.49±1.23	95.23±0.76	93.04±0.78	94.61±0.55	**97.30±0.37**
	87.30±1.30	95.69±0.53	95.66±0.96	96.16±0.63	**98.19±0.24**
GPDS	46.49±2.85	44.47±2.79	46.09±6.59	43.89±4.46	**49.11±2.42**
	52.80±3.95	55.73±2.04	55.10±2.82	55.50±2.62	**59.23±1.46**
	64.80±2.99	58.11±4.80	60.89±2.98	59.91±3.24	**65.06±1.98**
	69.20±2.76	63.10±1.41	65.43±3.01	64.33±2.26	**70.07±2.29**
CASIA	42.68±5.95	51.79±0.28	34.81±5.00	40.41±3.93	**53.87±0.07**
	56.81±4.31	63.28±2.62	56.28±6.52	49.70±5.72	**65.10±2.70**
	65.70±1.54	68.84±3.80	63.31±4.80	57.84±3.75	**69.71±3.64**
	66.45±5.83	69.57±2.55	69.33±4.74	58.64±4.67	**70.31±2.57**

palmprint recognition methods show good robustness to small-level Gaussian noise but not very good to high-level noise. However, it is obvious that the proposed method always achieves the highest accuracies among all the direction-based methods on all the noisy palmprint image datasets. Specially, when compared with the average accuracies of the four compared methods, the proposed method improves about 1% to 3% accuracy on the noisy PolyU database, and more than around 5% on noisy IITD, GPDS and CASIA databases, showing the effectiveness of the proposed method on noisy palmprint image recognition.

E. Intra-Comparison of LDDBP

It is seen that the proposed LDDBP method essentially consists of two discriminant direction components, namely, the LDDBP$_m$ and LDDBP$_s$, and each component includes three potential discriminant directions, namely, the first, second and last dominant directions. To further validate the effectiveness of the LDDBP and clarify the impact of its different components, we select different components as the features and compare them with the LDDBP in terms of the rank-one identification accuracy. Specifically, we respectively use the following direction representations to perform palmprint verification, including (1) the first dominant direction, (2) the combination of the first and second dominant directions, (3) the main discriminant direction group LDDBP$_m$, and (4) the secondary discriminant direction group LDDBP$_s$. Similarly, with the LDDBP, we use the blockwise histogram

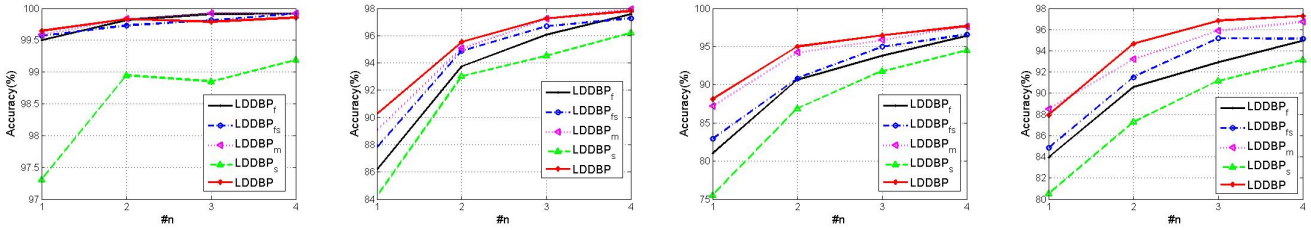

Fig. 10. The identification accuracies obtained based on different kinds of LDDBP-based descriptors on the (a)-(d) PolyU, IITD, GPDS and CASIA databases, respectively.

of the above four kinds of direction representations to form four kinds of local descriptors, which are referred to as LDDBP$_f$, LDDBP$_{fs}$, LDDBP$_m$, and LDDBP$_s$, respectively. In the matching stage, the Chi-square distance scheme is used. In this study, we also randomly selected 1 to 4 ($n = 1, 2, 3, 4$) images per palm as the training samples and the remaining are used as the query samples. We perform every LDDBP-based descriptor 10 times and calculate the average accuracies of them, as shown in Fig. 10. In addition, the accuracies obtained based on the LDDBP are also included in the figure for a better comparison.

From the comparative results, we can draw the following observations. First, the LDDBP$_{fs}$ performs better than the LDDBP$_f$. This result indicates that combining the first and second dominant directions definitely improve the discriminability of using the single most dominant direction feature. Second, the LDDBP$_m$ always outperforms the LDDBP$_{fs}$, confirming the high discriminability of the direction with the minimum convolved result. Third, the LDDBP$_m$ consistently outperforms the LDDBP$_s$ on the four palmprint databases, indicating that the LDDBP$_m$ has higher discriminative power than the LDDBP$_s$. The main reason lies in the fact that a number of points in a palmprint have no LDDBP$_s$. Fourth, the LDDBP generally outperforms the LDDBP$_m$. Exceptionally, the LDDBP$_m$ achieves a better performance than the LDDBP on the PolyU database. The possible reason is that the palmprint images of the PolyU database are contact-based captured, and thus these samples are high-quality and well-aligned. The LDDBP$_m$ has captured the most discriminative information, and the LDDBP$_s$ carries very few discriminative features that provides no helpful information to the LDDBP$_m$ for identification. Moreover, the LDDBP outperforms the LDDBP$_m$ on the other three palmprint databases, thereby validating the effectiveness of the LDDBP$_s$.

F. Discriminative Power of Different Directions

To compare the discriminability of different direction features, we respectively use different directions of a palmprint to perform palmprint identification. Specifically, twelve Gabor templates with different directions are used to extract the direction features. The direction index with the kth maximum filtering response, namely, the kth dominant direction, is selected as the feature code to form the blockwise descriptor. In the matching stage, the similar Chi-distance is used to measure the similarity of two direction-based descriptors. In this study, we randomly selected 4 samples from each palm to form the training sample set and use the remaining samples to form the test sample set. All the methods are repeated 10 times and the average identification accuracies are calculated. Moreover, for a dominant direction-based descriptor, the average accuracy (AVG) of the four databases is also calculated.

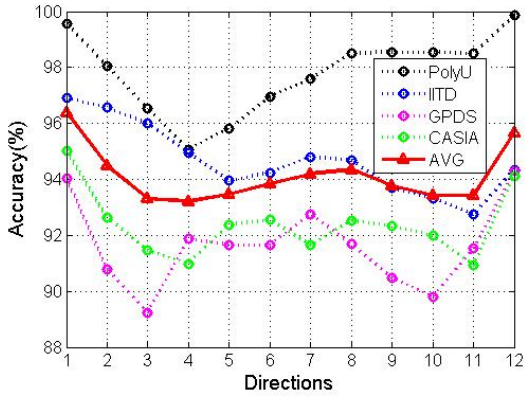

Fig. 11. The accuracies based on the different direction-based descriptors for the PolyU, IITD, GPDS and CASIA databases, respectively.

Fig. 11 depicts the accuracies obtained based on different dominant direction-based descriptors using the four databases, in which the index k on the $x-axis$ denotes the kth dominant direction. It can be seen that the accuracies along different directions are distributed such as the upside-down parabola-curves, which are consistent with the EGM. In general, the first, the last and the second dominant direction features usually have higher discriminability than the other directions. Therefore, the proposed method uses the first, second and last dominant directions to form the LDDBP descriptor.

G. The Optimal Local Block Size of LDDBP Descriptor

To overcome the small misalignment among ROIs, the proposed method uses the blockwise statistical feature to represent the exploited discriminant direction features. The conventional methods generally set the block size to 16×16 pixels. It is recognized that the optimal block size is highly related to the quality of the palmprint images. For example, for the palmprint images with serious misalignments after translation, a larger block size should be used, and otherwise a smaller block size should be set. To find the optimal local block size of the LDDBP descriptor, we conduct palmprint

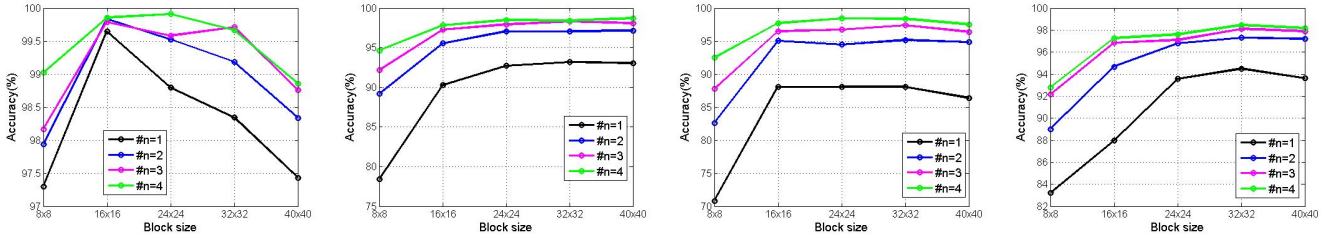

(a) (b) (c) (d)

Fig. 12. The identification accuracies based on the LDDBP descriptors with different local block sizes for the (a)-(d) PolyU, IITD, GPDS and CASIA databases, respectively.

identification based on the LDDBP descriptors using different block sizes, including 8×8, 16×16, 24×24, 32×32, and 40×40 pixels, respectively, and compare their performance. Similarly, 1 to 4 ($n = 1, 2, 3, 4$) palmprint images from each palm are selected as the training samples and the rest are used as the query samples. All the methods are repeated 10 times and the average identification accuracies are calculated. Fig. 12 depicts the identification results based on the different block sizes of the LDDBP.

From the comparative results, we see that a too small block size (i.e., 8×8 pixels) generally obtains a low accuracy since it cannot overcome the impact of misalignment. Furthermore, the LDDBP descriptors with the block sizes of 24×24 and 32×32 pixels can obtain the best performance on the IITD, GPDS, and CASIA databases. By contrast, for the PolyU database, the descriptor with the block size of 16×16 pixels achieves the highest accuracy. The possible reason is that the palmprint images in the PolyU database are acquired using a contact-based device with user-pegs with which the palms are generally aligned and the qualities of them are relatively higher. Therefore, here, a smaller local block size can better overcome the impact of the misalignment. Comparatively, the palmprint images in other three contactless databases have possible variations in their translations, rotations and scales, resulting in their serious misalignment. As a result, only a relatively larger block size can better fix the misalignment. Therefore, for contact-based palmprint images, the optimal block size should be approximately 16×16 pixels. For contactless palmprint images, the optimal block sizes are possibly from the 24×24 to 32×32 pixels.

H. Computational Time Cost Analysis

To evaluate the computational complexity of the proposed method, we calculated the computational time cost of the proposed method, and compared it with the representative direction-based methods. All algorithms were implemented on the same platform, a PC with double-core Intel(R) i5-3470(3.2GHz), RAM8.00GB, and MATLAB 12.0 under Windows10.0. We repeated all the algorithms 100 times and recorded the average time for both feature extraction and matching, as shown in Table III.

From the table, we see that the proposed LDDBP method takes a bit more time (about 0.04 s) than the competitive code and NDI methods, and it has comparable computational cost with the LLDP method. The main reason is that the most consuming computing of a direction-based method is the convolution operation in direction feature extraction. More filters used means more convolution calculation between images and filters. As a result, some methods using six filters, including the competitive code, ordinal code and NDI methods in feature extraction have relatively less computational cost. By contrast, the other methods, such as LDDBP and LLDP methods, adopting 12 filters in feature extraction have a litter more computational cost. Moreover, the proposed method uses more directions in optimal direction representation, resulting in more time taken than the LLDP methods. In addition, the feature matching time cost of most methods are less than 1 ms. Hence, the most time taken of palmprint recognition heavily depends on the feature extraction. We can also see that the total time cost of the proposed method is about 0.08 s in a whole process of palmprint verification, which can be acceptable in real-world applications.

TABLE III
THE AVERAGE TIME TAKEN (S) OF FEATURE EXTRACTION AND MATCHING IN A PALMPRINT VERIFICATION PROCESS USING DIFFERENT METHODS

	Feature extraction	Matching	Total
Competitive	0.0363	0.0004	0.0367
E-BOCV	0.0414	0.0009	0.0423
NDI	0.0396	0.0006	0.0402
ALDC	0.0785	0.0002	0.0787
LLDP	0.0742	0.0007	0.0749
LDDBP	0.0761	0.0007	0.0768

For palmprint identification, in practical applications, training is usually an offline process. That is, the feature extraction of training samples can be pre-performed offline, and thus, the matching time is our main concern. As shown in Table III, the proposed method has a fast matching speed (about 0.7 ms). Therefore, the computational complexity of our proposed method will not limit its practical applications.

V. CONCLUSION

In this paper, the essential connection between the discriminability of direction features and the direction feature extraction model is established, and a Gaussian-like model, namely, the EGM, is proposed to demonstrate the discriminative power of different directions. The EGM is suitable for both the single-dominant direction and multiple-dominant direction scenarios

in a palmprint and provides a new insight into the selection of discriminant direction features. Moreover, a novel local discriminant direction binary pattern is proposed to completely capture the direction features of a palmprint. Based on the EGM, three highly potential discriminant direction features are exploited from the LDDBP to form the LDDBP-based descriptor for palmprint recognition. The promising effectiveness of the proposed LDDBP method has been validated using four widely used palmprint image benchmarks. For future work, we are interested in extending the proposed method to other pattern recognition tasks, such as face- and texture-based image representation and recognition.

REFERENCES

[1] D. Zhang, *Advanced Pattern Recognition Technologies with Applications to Biometrics*. Hershey, PA, USA: IGI Globa, 2009.

[2] A. K. Jain, A. Ross, and S. Prabhakar, "An introduction to biometric recognition," *IEEE Trans. Circuits Syst. Video Technol.*, vol. 14, no. 1, pp. 4–20, Jan. 2004.

[3] A. K. Jain, K. Nandakumar, and A. Ross, "50 years of biometric research: Accomplishments, challenges, and opportunities," *Pattern Recognit. Lett.*, vol. 79, pp. 80–105, Aug. 2016.

[4] A. Kong, D. Zhang, and M. Kamel, "A survey of palmprint recognition," *Pattern Recognit.*, vol. 42, no. 7, pp. 1408–1418, 2009.

[5] E. Liu, A. K. Jain, and J. Tian, "A coarse to fine minutiae-based latent palmprint matching," *IEEE Trans. Pattern Anal. Mach. Intell.*, vol. 35, no. 10, pp. 2307–2322, Oct. 2013.

[6] L. Fei, G. Lu, W. Jia, J. Wen, and D. Zhang, "Complete binary representation for 3-D palmprint recognition," *IEEE Trans. Instrum. Meas.*, vol. 17, no. 12, pp. 2761–2771, Dec. 2018.

[7] D. Zhang, W. Zuo, and F. Yue, "A comparative study of palmprint recognition algorithms," *ACM Comput. Surv.*, vol. 44, no. 1, pp. 1–37, 2012.

[8] D. Zhong, X. Du, and K. Zhong, "Decade progress of palmprint recognition: A brief survey," *Neurocomputing*, to be published, doi: 10.1016/j.neucom.2018.03.081.

[9] L. Fei, G. Lu, W. Jia, S. Teng, and D. Zhang, "Feature extraction methods for palmprint recognition: A survey and evaluation," *IEEE Trans. Syst., Man, Cybern. Syst.*, to be published, doi: 10.1109/TSMC.2018.2795609.

[10] D.-S. Huang, W. Jia, and D. Zhang, "Palmprint verification based on principal lines," *Pattern Recognit.*, vol. 41, no. 4, pp. 1316–1328, 2008.

[11] D. Palma, P. L. Montessoro, G. Giordano, and F. Blanchini, "Biometric palmprint verification: A dynamical system approach," *IEEE Trans. Syst., Man, Cybern., Syst.*, to be published.

[12] A. Morales, M. A. Ferrer, and A. Kumar, "Towards contactless palmprint authentication," *IET Comput. Vis.*, vol. 5, no. 6, pp. 407–416, 2011.

[13] J. Dai and J. Zhou, "Multifeature-based high-resolution palmprint recognition," *IEEE Trans. Pattern Anal. Mach. Intell.*, vol. 33, no. 5, pp. 945–957, May 2011.

[14] S. Ribaric and I. Fratric, "A biometric identification system based on eigenpalm and eigenfinger features," *IEEE Trans. Pattern Anal. Mach. Intell.*, vol. 27, no. 11, pp. 1698–1709, Nov. 2005.

[15] H. Sang, W. Yuan, and Z. Zhang, "Research of palmprint recognition based on 2DPCA," in *Advances in Neural Networks*. Berlin, Germany: Springer, 2009, pp. 831–838.

[16] Z. Guo, G. Wu, Q. Chen, and W. Liu, "Palmprint recognition by a two-phase test sample sparse representation," in *Proc. Int. Conf. Hand-Based Biometrics*, 2011, pp. 1–4.

[17] L. Zhang, L. Li, A. Yang, Y. Shen, and M. Yang, "Towards contactless palmprint recognition: A novel device, a new benchmark, and a collaborative representation based identification approach," *Pattern Recognit.*, vol. 69, pp. 199–212, Sep. 2017.

[18] I. Rida, R. Herault, G. L. Marcialis, and G. Gasso, "Palmprint recognition with an efficient data driven ensemble classifier," *Pattern Recognit. Lett.*, to be published, doi: 10.1016/j.patrec.2018.04.033.

[19] I. Rida, S. Al-Maadeed, A. Mahmood, A. Bouridane, and S. Bakshi, "Palmprint identification using an ensemble of sparse representations," *IEEE Access*, vol. 6, pp. 3241–3248, 2018.

[20] D. Zhao, X. Pan, X. Luo, and X. Gao, "Palmprint recognition based on deep learning," in *Proc. ICWMMN*, 2015, pp. 214–216.

[21] S. Minaee and Y. Wang. (2016). "Palmprint recognition using deep scattering convolutional network." [Online]. Available: https://arxiv.org/abs/1603.09027

[22] M. Izadpanahkakhk, S. M. Razavi, M. Taghipour-Gorjikolaie, S. H. Zahiri, and A. Uncini, "Deep region of interest and feature extraction models for palmprint verification using convolutional neural networks transfer learning," *Appl. Sci.*, vol. 8, no. 7, p. 1210, 2018.

[23] W. Jia, R.-X. Hu, Y.-K. Lei, Y. Zhao, and J. Gui, "Histogram of oriented lines for palmprint recognition," *IEEE Trans. Syst., Man, Cybern., Syst.*, vol. 44, no. 3, pp. 385–395, Mar. 2014.

[24] D. Zhang, W.-K. Kong, J. You, and M. Wong, "Online palmprint identification," *IEEE Trans. Pattern Anal. Mach. Intell.*, vol. 25, no. 9, pp. 1041–1050, Sep. 2003.

[25] W. Jia *et al.*, "Palmprint recognition based on complete direction representation," *IEEE Trans. Image Process.*, vol. 26, no. 9, pp. 4483–4498, Sep. 2017.

[26] A. W.-K. Kong and D. Zhang, "Competitive coding scheme for palmprint verification," in *Proc. 17th Int. Conf. Pattern Recognit.*, 2004, pp. 520–523.

[27] W. Jia, D.-S. Huang, and D. Zhang, "Palmprint verification based on robust line orientation code," *Pattern Recognit.*, vol. 41, no. 5, pp. 1504–1513, 2008.

[28] L. Fei, Y. Xu, W. Tang, and D. Zhang, "Double-orientation code and nonlinear matching scheme for palmprint recognition," *Pattern Recognit.*, vol. 49, pp. 89–101, Jan. 2016.

[29] D. Hong, W. Liu, J. Su, Z. Pan, and G. Wang, "A novel hierarchical approach for multispectral palmprint recognition," *Neurocomputing*, vol. 151, pp. 511–521, Mar. 2015.

[30] A. Kong, D. Zhang, and M. Kamel, "Palmprint identification using feature-level fusion," *Pattern Recognit.*, vol. 39, no. 3, pp. 478–487, Mar. 2006.

[31] Y. Xu, L. Fei, J. Wen, and D. Zhang, "Discriminative and robust competitive code for palmprint recognition," *IEEE Trans. Syst., Man, Cybern., Syst.*, vol. 48, no. 2, pp. 232–241, Feb. 2018.

[32] Q. Zheng, A. Kumar, and G. Pan, "Suspecting less and doing better: New insights on palmprint identification for faster and more accurate matching," *IEEE Trans. Inf. Forensics Security*, vol. 11, no. 3, pp. 633–641, Mar. 2016.

[33] Z. Guo, D. Zhang, L. Zhang, and W. Zuo, "Palmprint verification using binary orientation co-occurrence vector," *Pattern Recognit. Lett.*, vol. 30, no. 13, pp. 1219–1227, 2009.

[34] L. Zhang, H. Li, and J. Niu, "Fragile bits in palmprint recognition," *IEEE Signal Process. Lett.*, vol. 19, no. 10, pp. 663–666, Oct. 2012.

[35] Z. Sun, T. Tan, Y. Wang, and S. Z. Li, "Ordinal palmprint represention for personal identification," in *Proc. IEEE Comput. Soc. Conf. Comput. Vis. Pattern Recognit. (CVPR)*, vol. 1, Jun. 2005, pp. 279–284.

[36] L. Fei, B. Zhang, Y. Xu, and L. Yan, "Palmprint recognition using neighboring direction indicator," *IEEE Trans. Human-Mach. Syst.*, vol. 46, no. 6, pp. 787–798, Dec. 2016.

[37] Y.-T. Luo *et al.*, "Local line directional pattern for palmprint recognition," *Pattern Recognit.*, vol. 50, pp. 26–44, Feb. 2016.

[38] L. Fei, J. Wen, Z. Zhang, K. Yan, and Z. Zhong, "Local multiple directional pattern of palmprint image," in *Proc. 23rd Int. Conf. Pattern Recognit. (ICPR)*, 2016, pp. 3013–3018.

[39] L. Fei, B. Zhang, S. Teng, and W. Zhang, "Local apparent and latent direction extraction for palmprint recognition," *Inf. Sci.*, vol. 473, pp. 59–72, Jan. 2019.

[40] G. Li and J. Kim, "Palmprint recognition with Local Micro-structure Tetra Pattern," *Pattern Recognit.*, vol. 61, pp. 29–46, Jan. 2017.

[41] T. Jabid, M. H. Kabir, and O. Chae, "Robust facial expression recognition based on local directional pattern," *ETRI J.*, vol. 32, no. 5, pp. 784–794, 2010.

[42] F. Zhong and J. Zhang, "Face recognition with enhanced local directional patterns," *J. Neurocomput.*, vol. 119, pp. 375–384, Nov. 2013.

[43] A. R. Rivera, J. R. Castillo, and O. O. Chae, "Local directional number pattern for face analysis: Face and expression recognition," *IEEE Trans. Image Process.*, vol. 22, no. 5, pp. 1740–1752, May 2013.

[44] N. Luo, Z. Guo, G. Wu, and C. Song, "Joint palmprint and palmvein verification by dual competitive coding," in *Proc. Int. Conf. Adv. Comput. Control (ICACC)*, 2011, pp. 538–542.

[45] T. Ojala, M. Pietikäinen, and T. Mäenpää, "Multiresolution gray-scale and rotation invariant texture classification with local binary patterns," *IEEE Trans. Pattern Anal. Mach. Intell.*, vol. 24, no. 7, pp. 971–987, Jul. 2002.

[46] *PolyU Palmprint Database*. Accessed: Jan. 1, 2004. [Online]. Available: http://www.comp.polyu.edu.hk/~biometrics/

[47] *IITD Touchless Palmprint Database*. Accessed: Jun. 10, 2008. [Online]. Available: http://www4.comp.polyu.edu.hk/čsajaykr/IITD/Database_Palm.htm
[48] *GPDS Palmprint Image Database*. Accessed: May 17, 2011. [Online]. Available: http://www.gpds.ulpgc.es
[49] *CASIA Palmprint Image Database*. Accessed: Jan. 1, 2005. [Online]. Available: http://biometrics.idealtest.org/
[50] A. Krizhevsky, I. Sutskever, and G. E. Hinton, "ImageNet classification with deep convolutional neural networks," in *Proc. Annu. Conf. Adv. Neural Inf. Process. Syst.*, 2012, pp. 1097–1105.
[51] K. Simonyan and A. Zisserman. (2014). "Very deep convolutional networks for large-scale image recognition." [Online]. Available: https://arxiv.org/abs/1409.1556
[52] K. He, X. Zhang, S. Ren, and J. Sun, "Deep residual learning for image recognition," in *Proc. IEEE Conf. Comput. Vis. Pattern Recognit. (CVPR)*, Jun. 2016, pp. 770–778.

Lunke Fei received the B.S. and M.S. degrees from East China Jiaotong University, China, in 2004 and 2007, respectively, and the Ph.D. degree in computer science and technology from the Harbin Institute of Technology, China, in 2016. He was with SIEMENS Ltd., and Nokia Siemens Networks, as a Software Engineer, from 2007 to 2013. He is currently an Associate Professor with the School of Computer Science and Technology, Guangdong University of Technology, Guangzhou, China. His research interests include biometrics, pattern recognition, image processing, and machine learning.

Bob Zhang (M'11) received the B.A. degree in computer science from York University, Toronto, ON, Canada, in 2006, the M.A.Sc. degree in information systems security from Concordia University, Montreal, QC, Canada, in 2007, and the Ph.D. degree in electrical and computer engineering from the University of Waterloo, Waterloo, ON, Canada, in 2011. After graduating from Waterloo, he remained with the Center for Pattern Recognition and Machine Intelligence, and later was a Post-Doctoral Researcher with the Department of Electrical and Computer Engineering, Carnegie Mellon University, Pittsburgh, PA, USA. He is currently an Assistant Professor with the Department of Computer and Information Science, University of Macau, Taipa, Macau. His research interests focus on biometrics, pattern recognition, and image processing. He is a Technical Committee Member of the IEEE Systems, Man, and Cybernetics Society, an Associate Editor of the *International Journal of Image and Graphics*, as well as an Editorial Board member of the *International Journal of Information*.

Yong Xu (M'06–SM'15) received the B.S. and M.S. degrees, and the Ph.D. degree in pattern recognition and intelligence system from the Nanjing University of Science and Technology, Nanjing, China, in 1994, 1997, and 2005, respectively. He is currently with the Bio-Computing Research Center, Harbin Institute of Technology, Shenzhen, China. His current research interests include pattern recognition, biometrics, bioinformatics, machine learning, image processing, and video analysis.

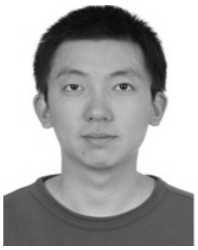

Di Huang (S'10–M'11) received the B.S. and M.S. degrees in computer science from Beihang University, Beijing, China, in 2005 and 2008, respectively, and the Ph.D. degree in computer science from the Ecole Centrale de Lyon, Lyon, France, in 2011. He then joined the Laboratory of Intelligent Recognition and Image Processing, School of Computer Science and Engineering, Beihang University, as a Faculty Member. He is currently an Associate Professor with Beihang University. His research interests include biometrics, 2-D/3-D face analysis, image/video processing, and pattern recognition.

Wei Jia (M'09) received the B.Sc. degree in informatics from Central China Normal University, Wuhan, China, in 1998, the M.Sc. degree in computer science from the Hefei University of Technology, Hefei, China, in 2004, and the Ph.D. degree in pattern recognition and intelligence system from the University of Science and Technology of China, Hefei, in 2008. He has been a Research Assistant, and also an Associate Professor with the Hefei Institutes of Physical Science, Chinese Academy of Science, from 2008 to 2016. He is currently a Research Associate Professor with the School of Computer and Information, Hefei University of Technology. His research interests include computer vision, biometrics, pattern recognition, image processing, and machine learning.

Jie Wen received the M.S. degree from Harbin Engineering University, China, in 2015. He is currently pursuing the Ph.D. degree in computer science and technology with the Shenzhen Graduate School, Harbin Institute of Technology, Shenzhen, China. His research interests include image and video enhancement, pattern recognition, and machine learning.